# Multiscale Mechanical Phenomena in Electrospun Carbon Nanotube Composites

## Ante Agic

*Faculty of Chemical Engineering and Technology, University of Zagreb, Zagreb, Croatia*

**ABSTRACT:** The carbon nanotube (CNT) structure is a promising building block for future nanocomposite structures. Mechanical properties of the electrospun butadiene elastomer reinforced with CNT are analyzed by multiscale method. Nanofiber diameter dependence on electric field and solution concentration is estimated from experimental data. The fiber microscale effective properties are determined by homogenization procedure using modified shear-lag model, while the point-bonded stochastic fibrous network on the mesoscale replaced by continuum effective sheet. Random fibrous network was generated according experimentally determined stochastic quantifiers. The influence of CNT reinforcement on elastic modulus of electrospun sheet on macroscopic level is determined by finite element method. © 2008 Wiley Periodicals, Inc. J Appl Polym Sci 108: 1191–1200, 2008

**Key words:** modeling; carbon nanotube; electrospinning; nanocomposites

## INTRODUCTION

The nanocomposites are expected to be a basic building element for future materials and structures. The carbon nanotubes (CNTs) have been proposed for many potential applications such as high-performance composites, electronic textile, sensors and nanoscale devices.[1] Polymer-CNT composites fascinate with unique mechanical, electrical, wide-range multifunctional properties. This has several significant implications; sensors made from nanofibers would be more sensitive to stimulants, composite made from nanofibers will be more efficient in transmitting its loads. The incorporation of CNTs into a polymer matrix can potentially provide structural materials with dramatically increased durability and strength. The addition of CNTs could increase glass transition, melting, and thermal decomposition temperatures of the polymer matrix. The interfacial bonding and proper dispersion of the CNTs in the polymer matrix are two main structural requirements. The interfacial shear strength and stress transfer depend on CNTs specific surface area and its chemical functionalization. On the other side, large CNTs surface area result with tendency to agglomerate, bundle together and entangle, what results many defect sites in the composites, and limiting the efficiency of CNTs on polymer matrices.[2] Today, the main challenges are to improve the dispersion and interface of CNTs in a polymer matrix when processing these nanocomposites.[3,4] The alignment of CNTs in a polymer matrix could be increased by *ex situ* alignment due to force, electrical, and magnetic field induced methods. Today, electrospinning has drawn considerable attention due to its uniqueness in producing CNT containing fibers with diameter smaller than 100 nm.[5] Electrospinning occurs when the electrical forces at the surface of a polymer solution overcome the surface tension and cause an electrically charged jet of polymer solution to be ejected. A schematic drawing of the electrospinning process is shown in Figure 1. The electrically charged jet undergoes a series of electrically induced instabilities during its passage to the collection surface which results in complicated stretching and looping of the jet.[6] This stretching process is accompanied by the rapid evaporation of the solvent molecules, further reducing the jet diameter. Dry fibers are accumulated on the surface of the collector, resulting in a nonwoven mesh of nanofibers. The process can be adjusted to control the fiber diameter by varying the processing parameters such as electric field strength, polymer solution concentration, and flow rate.[7] With an electric-field-controllable target electrode as a collector the alignment and dispersion has been improved.[8] This article is organized as follows. In section Material and Methods is given basic concepts of CNTs suspension electrospinning. Microscopic developments for embedding carbon nanotubes in the fibers together with macroscopic phenomena for fiber fabrics are discussed. Finally, in Results and Discussion are given same numerical and experimental results for this multiscale problem.

*Correspondence to:* A. Agic (aagic@marie.fkit.hr).
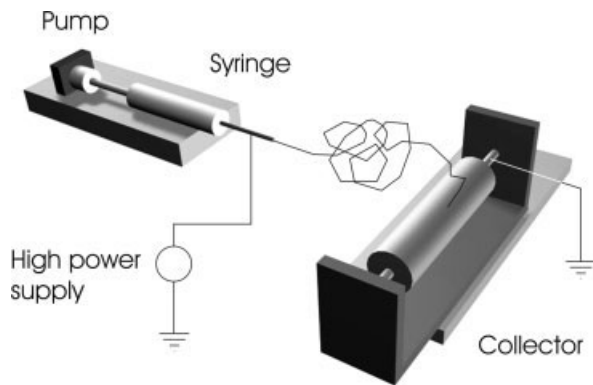
**Figure 1** The diagram of the electrospinning process.

## MATERIAL AND METHODS

### Experimental

The polymer, a syndiotactic 1-2 polybutadiene elastomer (JSR Co., Tokyo, Japan) has been used for this study. The carbon nanotube used in this work was vapor-grown carbon fibers. The CNTs were stirred in a ball mill for 2 h prior to being used. The elastomer was dissolved in chloroform. The voltage used was in the range 15–25 kV, and the distance between electrodes was 5–20 cm. The diameter of the fiber was measured by scanning electron microscope (Philips, Eindhoven, Holland). The wide-angle X-ray (WAXD) data were obtained using (Siemens, Karlsruhe, Germany) diffractometer. Tensile test was conducted on universal tensile test machine (Zwick, Ulm, Germany).

### Fundamentals of electrospinning

The slender-body approximation is widely used in electrospinning analysis. The replacement 3D axisymetric with 1D equivalent jet problem complicate carbon nanotube-fluid interaction forces on nanolevel domain. The applied electric field induced dipole moment, while torque on the dipole rotate and align the CNTs with electric field direction. The theories developed to describe the behavior of the suspension jet fall into two levels mesoscopic and microscopic. The mesoscopic governing equations of the electrospinning are equation of continuity, conservation of the charge, balance of momentum, and electric field equation.

Conservation of mass for the jet requires that[6,9]

$$\frac{\partial}{\partial t}\left(\pi \, r^2\right) + \frac{\partial}{\partial z}\left(\pi \, r^2 v\right) = 0 \quad (1)$$

where $r$ is jet radius, and $v$ is velocity. The conservation of charge may be expressed as

$$\frac{\partial}{\partial t}\left(2\pi r \mu\right) + \frac{\partial}{\partial z}\left(\pi \, r^2 KE + 2\pi r \mu\right) = 0 \quad (2)$$

where $E$ is the axial component of the electric field, $K$ is the electrical conductivity of the jet, and $\mu$ is the surface charge density. The momentum equation for the fluid can be derived as follows:

$$\rho\left(\frac{\partial v}{\partial t} + v\frac{\partial v}{\partial z}\right) = \rho \cdot g + \frac{\partial}{\partial z}\left(\tau_{zz} - \tau_{rr}\right) + \frac{\gamma}{r^2}\frac{\partial r}{\partial z}$$
$$+ \frac{\mu}{\varepsilon_0}\frac{\partial \mu}{\partial z} + (\varepsilon - \varepsilon_0)\cdot E\frac{\partial E}{\partial z} + \frac{2\mu}{r}E \quad (3)$$

where $\rho$ is fluid density, $\tau_{ij}$ is deviatoric stress tensor in fluid, $\gamma$ is the surface tension, and $\varepsilon$ and $\varepsilon_0$ are the dielectric constants of the jet and ambient air respectively. The equation for electric field has the form[6]

$$E = E_\infty - \left[\frac{1}{\varepsilon}\frac{\partial}{\partial z}(\mu \cdot r) - \frac{1}{2}\left(\frac{\varepsilon}{\varepsilon_0} - 1\right)\frac{\partial^2}{\partial z^2}(E \cdot r^2)\right] \cdot \ell n\left(\frac{L}{r_0}\right)$$
$$(4)$$

where $r_0$ is initial jet radius, $L$ is characteristic scale length, $E_\infty$ is the externally imposed constant electric field. For polymer suspension, stress tensor $\tau_{ij}$ come from polymeric $\hat{\tau}_{ij}$ and solvent contribution tensor via constitutive equation

$$\tau_{ij} = \hat{\tau}_{ij} + \eta_s \cdot \dot{\gamma}_{ij} \quad (5)$$

where $\eta_s$ is solvent viscosity and $\dot{\gamma}_{ij}$ strain rate tensor. The polymer contribution tensor $\hat{\tau}_{ij}$ depends on microscopic models of the suspension. Microscopic approach represents the microstructural features of material by means of a large number of micromechanical elements (beads, springs, rods) obeying stochastic differential equations. The evolution equations of the microelements arise from a balance of momentum on the elementary level. The rheological behavior of the dilute suspension of the CNTs in polymer matrix can be described as FENE dumbbell model[10]

$$\zeta\hat{\nabla}\langle Q \cdot Q\rangle = \delta_{ij} - \frac{c \cdot \langle Q.Q\rangle}{1 - tr\langle Q.Q\rangle/b_{max}} \quad (6)$$

where $\langle Q \cdot Q\rangle$ is the suspension configuration tensor, $c$ is a spring constant, and $b_{max}$ is maximum CNT extensibility. Symbol $\hat{\nabla}$ represent the upper convected derivative and $\zeta$ denote a relaxation time. The polymeric stress can be obtained from the following relation

$$\frac{\hat{\tau}_{ij}}{nkT} = \delta_{ij} - \frac{c\langle Q.Q\rangle}{1 - tr\langle Q.Q\rangle/b_{max}} \quad (7)$$

where $k$ is Boltzmann's constant, $T$ is temperature, and $n$ is dumbbells density. The jet originates from the tip of a cone like solution droplet similar to the Taylor cone. Initially the CNT is randomly oriented, but due flow in the spinneret cone, they are gradu-
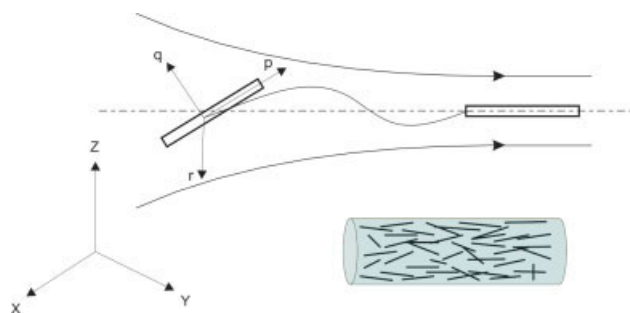
**Figure 2** The CNTs alignment in jet flow. [Color figure can be viewed in the online issue, which is available at www.interscience.wiley.com.]

ally oriented along the streamline (see Fig. 2). Rotation motion of a CNTs in a Newtonian flow can be described as short fiber suspension model as another rheological model[11]

$$\frac{dp}{dt} = \frac{1}{2} w_{ij} p_j + \frac{1}{2} \Theta \left( \frac{d\gamma_{ij}}{dt} p_j - \frac{d\gamma_{kl}}{dt} p_k p_l p_i \right) - D_r \frac{1}{\psi} \frac{\partial \psi}{\partial t}. \quad (8)$$

where $p$ is a unit vector in CNT axis direction, $\omega_{ij}$ is the rotation rate tensor, $\gamma_{ij}$ is the deformation tensor, $D_r$ is the rotary diffusivity, and $\Theta$ is shape factor. Orientation probability distribution function $\psi$ can be described by the Fokker-Planck equation

$$\frac{\partial \psi}{\partial t} + \frac{\partial}{\partial p} (\psi \cdot p) = D_r \nabla^2 \psi \quad (9)$$

Microscopic models for evolution of suspension microstructure can be coupled to macroscopic transport equations of mass and momentum to yield micro–macro models.[11] The micro–macro approach couples the mesoscopic scale of kinetic theory to the macroscopic scale continuum mechanics. The presence of the CNTs in the solution contributes to new form of instability with influences on the formation of the electrospun mat. The high strain rate on the nanoscale with complicated microstructure requires innovative research approach from the computational modeling point of view. The CNTs suspension can be described as system consists from a Smoluchowski equation for the orientation distribution function of the nano-rods together with Navier-Stokes equation for the solvent with an orientation-dependent stress.[12]

## Microscopic properties

The fiber morphology strongly dependent on important electrospinning processing parameters that affect on and diameter of produced fibrous structure has been identified by many researches.[5,6] The solution concentration, electric field, spinning distance, polymer viscosity are some of them. The CNT have

the large aspect ratio (length/radii) beneficial to their use in composite. Using response surface methodology,[13] mean fiber diameter dependence on electric field and solution concentration can be approximated by a second-order polynomial model

$$d = A_{00} + A_{01} \cdot \hat{c} + A_{02} \cdot \hat{c}^2 + A_{10} \cdot \hat{V} + A_{11} \cdot \hat{c} \cdot \hat{V} + A_{20} \cdot \hat{V}^2$$
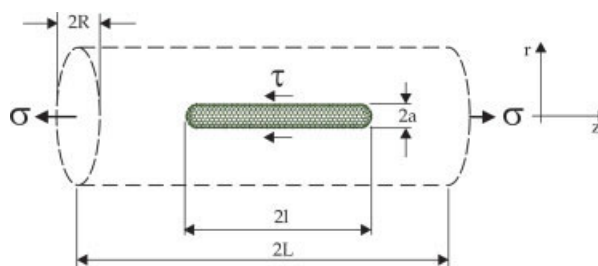
$$\hat{c} = \frac{c - \frac{1}{2}(c_{min} + c_{max})}{\frac{1}{2}(c_{min} - c_{max})}, \quad \hat{V} = \frac{V - \frac{1}{2}(V_{min} + V_{max})}{\frac{1}{2}(V_{min} - V_{max})} \quad (10)$$

where $\hat{c}$ and $\hat{V}$ are nondimensional solution concentration and nondimensional electric field, respectively. The numerical values of the coefficients $A_{00}, A_{01}, A_{02}, A_{10}, A_{11}, A_{20}$ are determined by nonlinear regression analysis, fitting surface defined by eq. (10) across experimental data points. To characterize the macroscopic properties of the fibrous structure, the effective properties of the nanofiber on microscale must be prior determined. The effective properties of the nanofiber can be determined by homogenization procedure using representative volume element (RVE). It is necessary to incorporate more physical information on microscale in order to precise determine material behavior model. A concentric composite cylinder embedded with a caped carbon nanotube represents RVE shown on Figure 3. A carbon nanotube with the length $2\ell$, radius $a$ is embedded at the centre of matrix materials with the radius $R$ and the length $2L$.

The discrete atomic nanotube structure replaced the effective (solid) fiber having the same length and outer diameter as a discrete nanotube with effective Young's nanotube modulus is determined from atomic structure.[14] The stress transfer between fiber and matrix in RVE is determined using modified shear-lag model.[15] The governing equations for the axisymmetric problem are

$$\frac{\partial \sigma_{rr}}{\partial r} + \frac{\partial \tau_{rz}}{\partial z} + \frac{\sigma_{rr} - \sigma_{\theta\theta}}{r} = 0$$
$$\frac{\partial \tau_{rz}}{\partial r} + \frac{\partial \sigma_{zz}}{\partial z} + \frac{\tau_{rz}}{r} = 0 \quad (11)$$



**Figure 3** The nanofiber representative volume element. [Color figure can be viewed in the online issue, which is available at www.interscience.wiley.com.]

In eqs. (11) $\sigma_{rr}$, $\sigma_{\theta\theta}$, $\sigma_{zz}$, and $\tau_{rz}$ are stress tensor components. The boundary conditions for this problem of axially loaded fiber, are given by

$$t^m_{r=R} = 0$$
$$t^m_{z=\pm L} = \pm\sigma_o \qquad (12)$$

where $t$ is the traction vector, $\sigma_o$ was the axial normal stress uniformly applied on $z = \pm L$. The superscripts $m$ and $f$ denote the matrix and fiber, respectively (see Fig. 3). Using Hook's law as constitutive equations between stress and strain

$$\varepsilon_{rr} = \frac{1}{E}[\sigma_{rr} - v(\sigma_{\theta\theta} + \sigma_{zz})]$$
$$\varepsilon_{zz} = \frac{1}{E}[\sigma_{zz} - v(\sigma_{rr} + \sigma_{\theta\theta})] \qquad (13)$$
$$\gamma_{rz} = \frac{\tau_{rz}}{G}$$

and kinematics relationship between strain and displacement,

$$\varepsilon_{rr} = \frac{\partial u}{\partial r} \qquad \varepsilon_{zz} = \frac{\partial w}{\partial z} \qquad \gamma_{rz} = \frac{\partial u}{\partial z} + \frac{\partial w}{\partial r} \qquad (14)$$

the solution of the above given equations yields distribution stress and strain components under RVE. The $\varepsilon_{rr}$, $\varepsilon_{\theta\theta}$, $\varepsilon_{zz}$, and $\gamma_{rz}$ are stain tensor components, $u$ and $w$ are radial and axial displacement vector components, $E, v,$ and $G$ are, the Young's modulus, Poisson's ratio, and shear modulus of the material, respectively. For example, in the region $-\ell \leq z \leq \ell$ axial component of stress tensor (dimensionless form) for fiber and matrix has the following form

$$\frac{\sigma^m_{zz}}{\sigma_o} = \frac{\ln\frac{r}{a} - \frac{1}{2}\left(\frac{r^2}{R^2} - \frac{a^2}{R^2}\right)}{\ln\frac{R}{a} - \frac{1}{4}\left(1 - \frac{a^2}{R^2}\right)\left(3 - \frac{a^2}{R^2}\right)} + \left\{\frac{E_m}{E_f} - \frac{\left[\frac{a^2}{R^2} + \frac{E_m}{E_f}\left(1 - \frac{a^2}{R^2}\right)\right]\left[\ln\frac{r}{a} - \frac{1}{2}\left(\frac{r^2}{R^2} - \frac{a^2}{R^2}\right)\right]}{\ln\frac{R}{a} - \frac{1}{4}\left(1 - \frac{a^2}{R^2}\right)\left(3 - \frac{a^2}{R^2}\right)}\right\} \bullet$$

$$\bullet \left\{\frac{1}{\frac{a^2}{R^2} + \frac{E_m}{E_f}\left(1 - \frac{a^2}{R^2}\right)} + \left[1 - \frac{1}{\frac{a^2}{R^2} + \frac{E_m}{E_f}\left(1 - \frac{a^2}{R^2}\right)}\right]\frac{\cosh(\kappa z)}{\cosh(\kappa \ell_0)}\right\}$$

$$\frac{\sigma^f_{zz}}{\sigma_o} = \frac{1}{\frac{a^2}{R^2} + \frac{E_m}{E_f}\left(1 - \frac{a^2}{R^2}\right)} + \left[1 - \frac{1}{\frac{a^2}{R^2} + \frac{E_m}{E_f}\left(1 - \frac{a^2}{R^2}\right)}\right]\frac{\cosh(\kappa z)}{\cosh(\kappa \ell_0)} \qquad (15)$$

The shear-lag parameter[14] $\kappa$ has the following form

$$\kappa^2 = \frac{1}{1 + v_m}\frac{1}{R^2}\left[\left(\frac{R}{a}\right)^2 - 1\right]\frac{\left[\left(\frac{a}{R}\right)^2 + \frac{E_m}{E_f}\left(1 - \frac{a^2}{R^2}\right)\right]}{\ln\frac{R}{a} - \frac{1}{4}\left(1 - \frac{a^2}{R^2}\right)\left(3 - \frac{a^2}{R^2}\right)}$$

For the known stress and strain distribution under RVE, we can calculate elastic effective properties quantifiers. The effective axial module $E_{zz}$ and the transverse module $E_{xx} = E_{yy}$ can be calculated as follows:

$$E_{zz} = \frac{\langle\sigma_{zz}\rangle}{\langle\varepsilon_{zz}\rangle}$$
$$E_{xx} = \frac{\langle\sigma_{xx}\rangle}{\langle\varepsilon_{xx}\rangle} \qquad (16)$$

where $\langle\ \rangle$ denotes a volume average under volume $V$ as defined by

$$\langle\Xi\rangle = \frac{1}{V}\int_v \Xi(x,y,z).dV$$

The Poisson's ratio is obtained in the same way, for example

$$v_{xy} = \frac{\langle\varepsilon_{yy}\rangle}{\langle\varepsilon_{xx}\rangle} \qquad (17)$$

The same can be said for all remaining effective properties. It is possible in this model to extend to damage and interphase bonding.[16] In all above analyses, CNT is treated as a straight tube, but in reality, CNT has the form of the curved tubes (see Fig. 2). The CNTs concentration increase, the surface of the fibers becomes rougher with local no uniformities with tendency of the agglomerations. The nanotube waviness reduces the effective modulus of the composite relative to straight nanotube reinforcement.[17] The large deformation extensibility and resilience of elastomeric matrix, fiber stress-strain constitutive model require the strain energy density concept use. In framework anisotropic hyperelastic material, the strain energy of the fiber as composite, $U$ can be described as[18]

$$U = \left(1 - \sum_i f_i\right) \cdot U_{matrix}(I_1, I_2, I_3) + \sum_i f_i \cdot U_{CNT}(I_{4i}, I_{5i}, I_3)$$

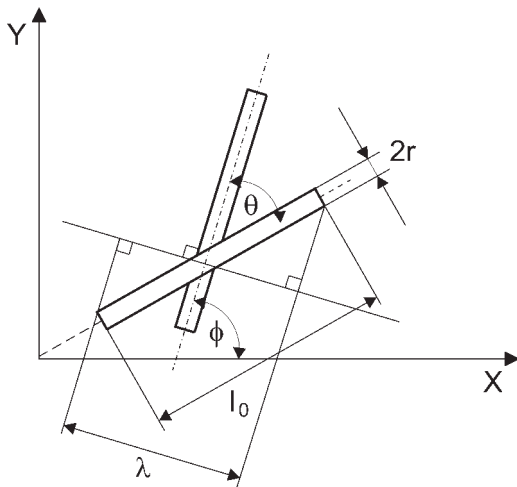$$I_{4i} = a_i \cdot C \cdot a_i, \qquad I_{5i} = a_i \cdot C^2 \cdot a_i \qquad (18)$$

**Figure 4** The fiber contact analysis.

Here, we assume a simple rule of mixture approach is valid.[18] The $f_i$ is the volume fraction of CNTs aligned in the $i$-th direction, where $I_1, I_2, I_3$ are invariants of the right Cauchy-Green tensor of deformation $C_{ij}$. The CNTs stain energy contribution can be expressed as sum all CNT fibers with orientation $a_i$, depend on invariant $I_{4i}$ and $I_{5i}$ as square of the CNTs stretch in $i$-th direction. Therefore, fourth-order elastic tensor for the fiber has the following form

$$D_{ijkl} = 4 \cdot \sum_n \sum_m \left( \frac{\partial^2 U}{\partial I_n \partial I_m} \frac{\partial I_n}{\partial C_{ij}} \otimes \frac{\partial I_m}{\partial C_{kl}} + \frac{\partial U}{\partial I_n} \frac{\partial^2 I_n}{\partial C_{ij} \partial C_{kl}} \right) \quad (19)$$

## Network macroscopic properties

The major objective in the determination of macroscopic properties is the link between atomic and continuum types of modeling and simulation approaches. The multiscale method such as quasi-continuum, bridge method, coarse-grain method, and dissipative particle dynamics are some popular mesoscale methods.[14] Each CNT is represented as a chain of connected dissipative particles or flexible cylinders.[19] The main advantage of the mesoscopic model is its higher computational efficiency than the molecular modeling without a loss of detailed properties at molecular level. Peridynamic modeling of fibrous network is another promising method, which allows damage, fracture and long-range forces to be treated as natural components of the deformation of materials.[20] In this article, the macroscopic material properties are determined by multiscale modelling approach. In the first stage, effective fiber properties are determined by homogenization procedure using modified shear lag model, while in the second stage the point-bonded stochastic fibrous network at meso-scale is replaced by continuum plane stress model.

Effective mechanical properties of nanofiber sheets at the macro scale level can be determined using the 2D Timoshenko beam-network. The critical parameters are the mean number of crossings per nanofiber, total nanofiber crossing in sheet and mean segment length.[21] Let us first consider a general planar fiber network characterized by fiber concentration $n$ and fiber angular and length distribution $\psi(\phi, \ell)$, where $\phi$ and $\ell$ are fiber orientation angle and fiber length, respectively. The fiber radius $r$ is considered uniform and the fiber concentration $n$ is defined as the number of fiber per unit area. We assumed that $\phi$ and $\ell$ are uncorrelated, thus it can be written as

$$\psi(\phi, \ell) = \psi_1(\phi) \cdot \psi_2(\ell) \quad (20)$$

The Poisson probability distribution can be used to describe the fiber segment lenght distribution for electrospun fabrics,[22] a portion of the fiber between two neighboring contacts:

$$f(\ell) = \frac{1}{\bar{\ell}} \exp(-\ell/\bar{\ell}) \quad (21)$$

where $\bar{\ell}$ is the mean segment length. For fiber network made of fibers with uniform lengths $\ell_0$, number of intersecting fibers with fixed fiber, within an area $\lambda(\vartheta) \cdot \ell_0 + 2r \cdot \ell_0$ can be estimated as (Fig. 4)

$$dN = n \cdot [\ell_0 \cdot \lambda(\vartheta) + \ell_0 \cdot 2r] \cdot \psi(\vartheta, \ell) \cdot d\ell \cdot d\vartheta \quad (22)$$
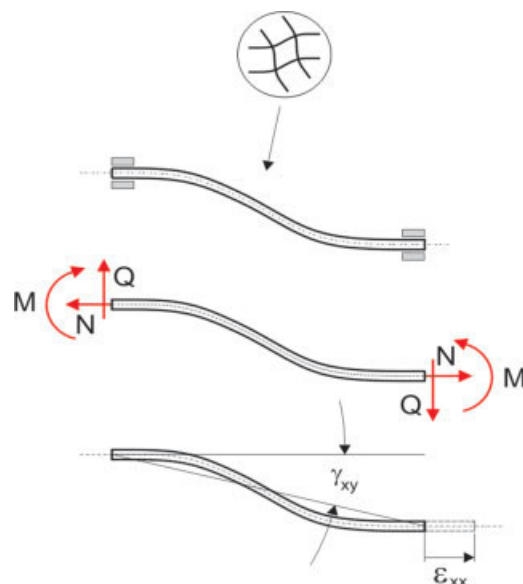


**Figure 5** Fiber network 2D model. [Color figure can be viewed in the online issue, which is available at www.interscience.wiley.com.]
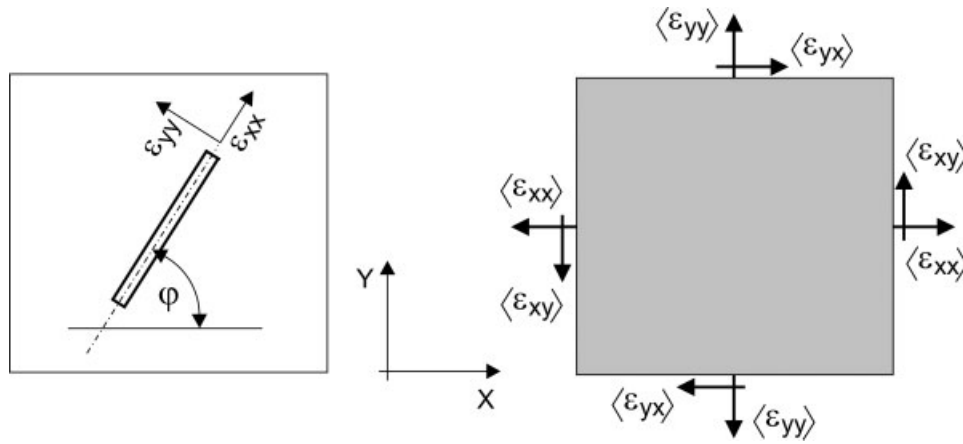
**Figure 6** The micro-macro affine transformation.

where $\lambda(\vartheta)$ is the projected length of the fixed fiber on a straight line perpendicular to the fiber with orientation $\phi$. Integrating the above relation over all possible fiber length and orientations yields the average contact number per fiber. The total number fiber segments $\hat{N}$ in the rectangular region $b \times h$ can be determined according to

$$\widehat{N} = \{n \cdot \ell_0 (\langle\lambda\rangle + 2r) - 1\} \cdot n \cdot b \cdot h \qquad (23)$$

with

$$\langle\lambda\rangle = \int_0^\phi \int_0^\infty \psi(\vartheta, \ell) \cdot \lambda(\vartheta) \cdot d\ell \cdot d\vartheta$$

where the dangled segments at fiber ends have been excluded.

The fiber network will be deformed in several ways. The strain energy in fiber segments come from bending, stretching, and shearing modes of deformation (see Fig. 5)

$$U = n \cdot \ell_0 \cdot b \cdot h \int \int \frac{1}{2} \frac{E \cdot A}{\ell} \varepsilon_{xx}^2 \cdot \psi(\phi, \ell) \cdot \ell \cdot d\ell \cdot d\phi$$
$$+ n \cdot \{n \cdot \ell_0 \cdot (\langle\lambda\rangle + 2r) - 1\} \cdot b \cdot h \cdot$$
$$\times \left\{ \int \int \frac{1}{2} \frac{G \cdot A}{\ell} \cdot \gamma_{xy}^2 \cdot \psi(\phi, \ell) \cdot \ell \cdot d\ell \cdot d\phi \right.$$
$$\left. + \int \int \frac{1}{2} \cdot \frac{3 \cdot E \cdot I}{\ell^3} \gamma_{xy}^2 \cdot \psi(\phi, \ell) \cdot \ell \cdot d\ell \cdot d\phi \right\} \quad (24)$$

where $A$ is fiber cross-section area and $I$ is fiber cross-section moment of inertia.

The effective material constants for fiber network can be determined using homogenization procedure concept for fiber network. The strain energy fiber network for representative volume element is equal to strain energy continuum element with effective material constant (see Fig. 6). The strain energy of the representative volume element under plane stress conditions are
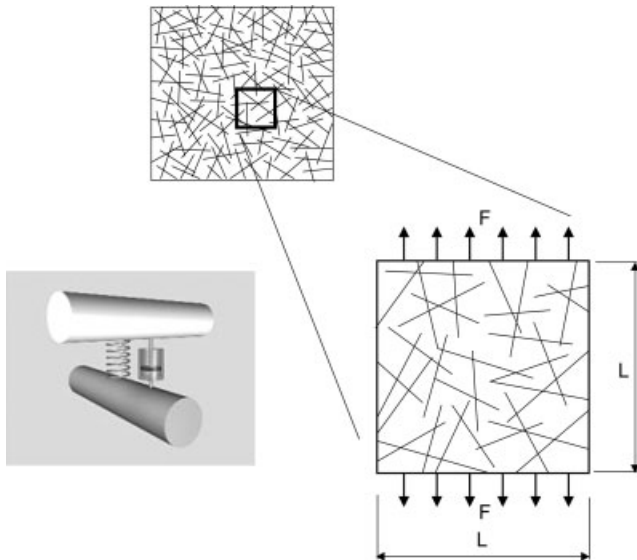


**Figure 7** The finite element model of the fiber net.
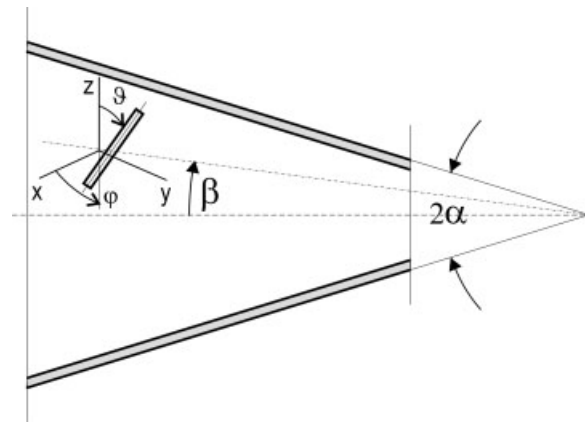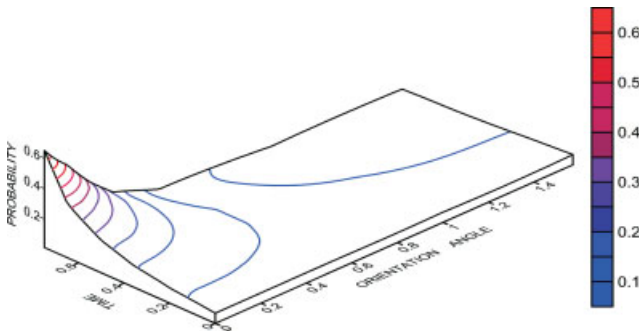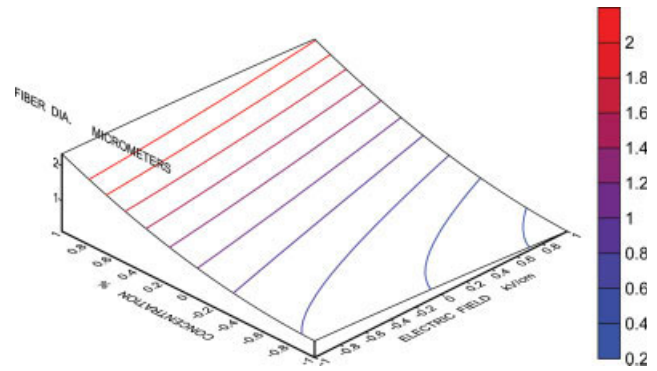


**Figure 8** Hamel flow.

**Figure 9** Probability distribution function dependence on time and orientation. [Color figure can be viewed in the online issue, which is available at www.interscience.wiley.com.]



**Figure 10** Fiber diameter dependence on solution concentration and electric field. [Color figure can be viewed in the online issue, which is available at www.interscience.wiley.com.]

$$U = \frac{1}{2} \begin{Bmatrix} \langle \varepsilon_{xx} \rangle \\ \langle \varepsilon_{yy} \rangle \\ \langle \gamma_{xy} \rangle \end{Bmatrix}^{T} \frac{1}{1 - v_{12}v_{21}}$$

$$\times \begin{bmatrix} E_1 & E_1 v_{21} & 0 \\ E_1 v_{12} & E_2 & 0 \\ 0 & 0 & G_{12}(1 - v_{12}v_{21}) \end{bmatrix} \begin{Bmatrix} \langle \varepsilon_{xx} \rangle \\ \langle \varepsilon_{yy} \rangle \\ \langle \gamma_{xy} \rangle \end{Bmatrix} \cdot V \quad (25)$$

where $V = b \cdot h \cdot 2 \cdot r$ is representative volume element, $E_1, E_2, G_{12}, v_{12}$ are effective material constants. The square bracket $\langle \varepsilon_{ij} \rangle$ means macroscopic strain value. We assume that microscopic deformation tensor of a fiber segments $\varepsilon_{ij}$ is compatible with effective macroscopic strain $\langle \varepsilon_{ij} \rangle$ of effective continuum, and therefore we can write

$$\varepsilon_{xx} = \frac{1}{2} \left[ \langle \varepsilon_{xx} \rangle + \langle \varepsilon_{yy} \rangle \right] + \frac{1}{2} \left[ \langle \varepsilon_{xx} \rangle + \langle \varepsilon_{yy} \rangle \right] \cos 2\phi$$
$$+ \langle \varepsilon_{xy} \rangle \sin 2\phi$$
$$\varepsilon_{xy} = -\frac{1}{2} \left[ \langle \varepsilon_{xx} \rangle - \langle \varepsilon_{yy} \rangle \right] \sin 2\phi + \langle \varepsilon_{xy} \rangle \cos 2\phi \quad (26)$$

This is bridge relations between fiber segment microstrain $\varepsilon_{ij}$ and macroscopic strain $<\varepsilon_{ij}>$ in the effective medium.

### Finite element method

Effective mechanical properties of nanofiber sheets at the macro scale level can be determined using the 2D Timoshenko beam-network. Properties of this nanofibrous structure on the macro scale depend on the 3D joint morphology. The joints can be modeled as contact elements with spring and dashpot.[21] The elastic energy of the whole random fiber network can be calculated numerically, from the local deformation state of the each segment by finite element method.[23] For the random point field, the stochastic

fiber network was generated. The nonload bearing fiber segments were removed and trimmed to keep dimensions $L \times L$ of the representative window (see Fig. 7). A line representative network model is replaced by finite element beam mesh. The number of intersections/unit area and mean lengths are obtained from image analysis of electrospun sheets. The elastic energy of the network is then the sum of the elastic energies of all segments. We consider here tensile stress, and the fibers are rigidly bonded to each other at every fiber–fiber crossing points. The finite element analyses were performed in a network of 100 fibers, for some CNTs volume fractions values. Nanofibers were modeled as equivalent cylindrical beam as mentioned above. The problem is reduced to the solution of the linear system of equations

$$[K_e] \cdot \{u\} = \{f\} \quad (27)$$

where are $\{u\}$ is global displacement vector, $\{f\}$ is global nodal force vector, and $[K_e]$ is global stiffness matrix.
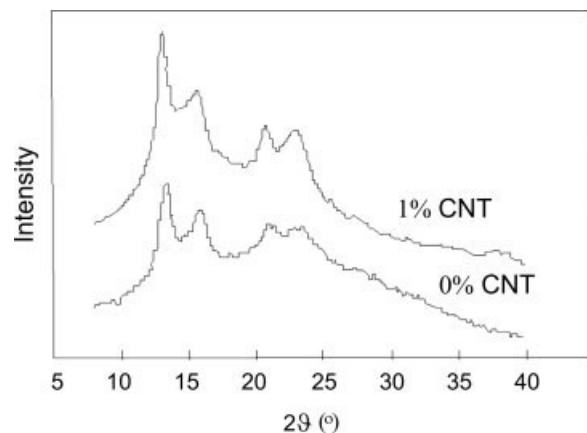


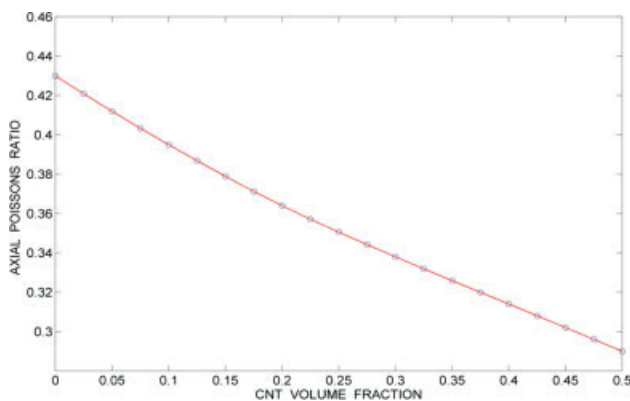**Figure 11** X-ray spectrum for CNTs composites.
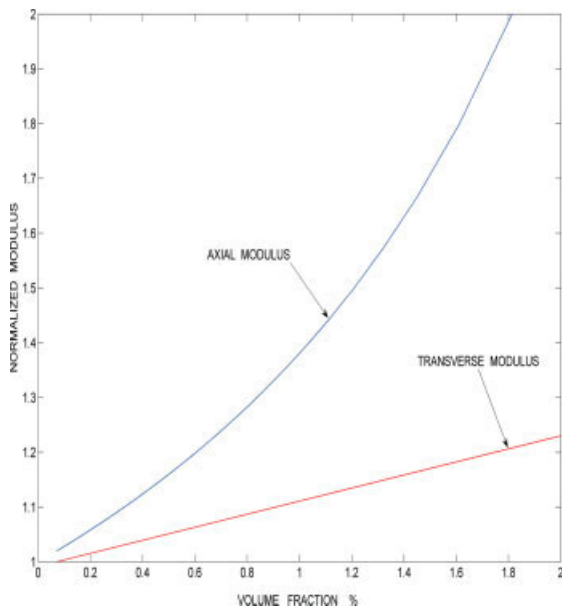
Figure 12 The effective modulus dependence on CNTs contents. [Color figure can be viewed in the online issue, which is available at www.interscience.wiley.com.]

## RESULTS AND DISCUSSION

The quality of the nanofiber depends on the carbon nanotube distribution and alignments during electrospinning. A simple model describing the flow of CNT dispersed elastomer solution is planar sink flow in the cone, known as the Hamel flow. For the Hamel flow the nonzero velocity component is radial

$$v_r = \frac{v}{r} F(\beta) \tag{28}$$

where $v$ is the kinematics viscosity of the fluid. The function $F(\beta)$ is found as a solution of the Navier-Stokes equations in the approximate form[23]



Figure 13 The effective axial Poisson's ratio dependence on CNTs contents. [Color figure can be viewed in the online issue, which is available at www.interscience.wiley.com.]
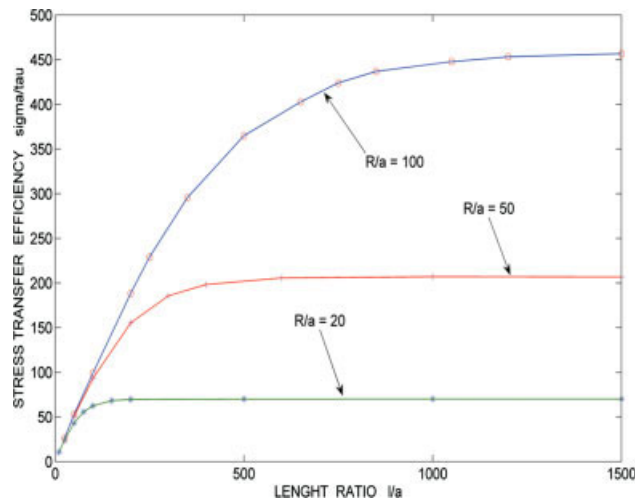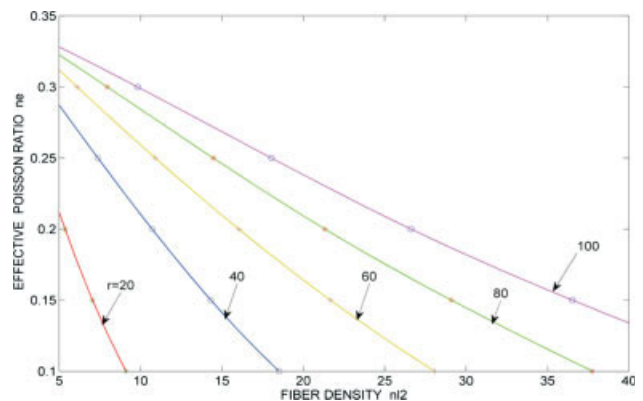
Figure 14 The stress transfer efficiency. [Color figure can be viewed in the online issue, which is available at www.interscience.wiley.com.]

$$F(\beta) = \Re e \left\{ 3 \tanh^2 \left[ \left( -\frac{1}{2} \Re e \right)^{1/2} (\alpha - \beta) + \gamma \right] - 2 \right\}$$

$$\gamma = \tanh^{-1} \left( \frac{2}{3} \right)^{1/2} \tag{29}$$

Solution eqs. (28) and (29) for Hamel flow in the cone (see Fig. 8), give the value of the orientation probability distribution function $\psi$ along streamline. For the stream line defined by the angle $\beta = \alpha/5$, $\alpha = 60°$, dependence function $\psi$ on dimensionless time and angular position are shown on Figure 9. The Reynolds number was chosen to be $\Re e = 50$.

Experimental data for fiber diameter produced fibrous structure depending on solution concentration and electric field have been identified. The coefficient in second-order model [eq. (10)] determined by multiple regression analysis using experimental data



Figure 15 The effective Poisson's ratio dependence on fiber density $n \cdot \ell_0^2$ and aspect ratio $\ell_0/r$. [Color figure can be viewed in the online issue, which is available at www.interscience.wiley.com.]
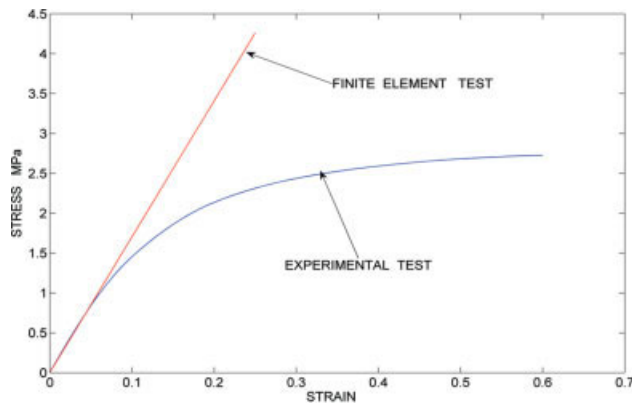
**Figure 16** The stress-strain curve. [Color figure can be viewed in the online issue, which is available at www. interscience.wiley.com.]

for electrospinning CNT-butadiene elastomer solution. For a quadratic model and two factors, we need nine possible combinations of factor settings. The contour plots suggesting that the lower concentration together with electric field increase gives lower fiber diameter. The stationary point is minimum values of the response or the smallest fiber diameter. The surface contours plots of these parameters outline the optimum condition for electrospinning (see Fig. 10).

The WAXD profile of the CNT/elastomer system is shown in Figure 11. The position at maximum intensity of the diffraction angles, $2\vartheta$ for the four peaks corresponds to the spacing of 0.65, 0.55, 0.41, and 0.38 nm, respectively. The WAXD profile is influ-

enced by presence of CNTs in system, as crystal structure changes with presence of CNTs.

The matrix material was considered to be butadiene elastomer, with $E_m = 8\ MPa$ and $v_m = 0.43$.[24] The CNT were considered to be isotropic with $E_f = 545\ GPa$ and $v_f = 0.3$.[25] The effective axial modulus in dimensionless form $\langle E_{zz}\rangle/E_m$, and the transverse modulus $\langle E_{xx}\rangle/E_m$ on micro level, for the range of volume CNTs fractions are shown in Figure 12. The $\langle E_{xx}\rangle$ is greatly influenced by the presence of CNTs, while $\langle E_{yy}\rangle$ is insensitive to CNTs, due to the matrix presence three orders smaller modulus. The Poisson's ratio indicates similar behavior trend. The effective axial Poisson's ratio is shown in Figure 13.

The ratio between maximum normal stress $\sigma_{max}$ and maximum shear stress $\tau_{max}$, $\delta = \sigma_{max}/\tau_{max}$, is of great importance among many others. This parameter $\delta$ characterizes the efficiency of transferring shear stress into tensile stress through a tube-matrix interface. Figure 14 shows the variation of $\delta$ with the tube aspect ratio $\ell/a$ and nanotube volume fraction $R/a$. The large $\delta$ allows a high tensile stress to be obtained at a relatively low shear stress level, to reduce the possibility of matrix failure.

The influence of two macroscopic parameters on effective properties is illustrated by Figure 15. The Figure 15 shows the effective Poisson ratio sheets dependence on fiber concentration $n\ell_0^2$ and fiber aspect ratio $\ell_0/r$. For random planar network, i.e., $\psi_1(\phi) = \frac{1}{\pi}$, the effective Young modulus $\langle E\rangle$, and Poisson ratio $\langle v\rangle$, after homogenization procedure have the following form

$$\frac{\langle E\rangle}{E_m} = \pi\left(1 - \langle v\rangle^2\right)\cdot\left(n\cdot\ell_0^2\right)\cdot\frac{r}{\ell_0}\left\{\frac{3}{16} + 2\cdot\left[\left(n\cdot\ell_0^2\right)^2\cdot\left(\frac{1}{\pi} + \frac{r}{\ell_0}\left(1 + \frac{2}{\pi}\right)\right)^2 - \frac{1}{4}\right]\cdot\left(\frac{\xi}{1+v} + \zeta\right)\right\}$$

$$\langle v\rangle = \frac{\pi^2 - 32\cdot\left\{\left(n\cdot\ell_0^2\right)^2\left[\frac{1}{\pi} + \left(1 + \frac{2}{\pi}\right)\cdot\frac{r}{\ell_0}\right] - \frac{1}{4}\right\}\left(\frac{\xi}{1+v} + \zeta\right)}{3\cdot\pi^2 + 32\cdot\left\{\left(n\cdot\ell_0^2\right)^2\left[\frac{1}{\pi} + \left(1 + \frac{2}{\pi}\right)\cdot\frac{r}{\ell_0}\right] - \frac{1}{4}\right\}\left(\frac{\xi}{1+v} + \zeta\right)}$$

$$\xi = \frac{1}{4(N+1)^2}\int_0^{\ell_0} x\exp(-x)\cdot dx, \quad \zeta = \frac{3r^2}{2\ell_0^2}\int_0^{\ell_0}\frac{1}{x}\exp(-x)\cdot dx \tag{30}$$

where $E_m$ is fiber matrix modulus.

Finite element analyses were performed for computer generated network of 100 fibers. The comparison of calculated data with experimental data for nanotube sheet shows some discrepancies (Fig. 16). A rough morphological network model for the sheets can explain this on the one hand and simple joint morphology on the other hand.[22,26] The finite element program should be extending to large displacement and deformation. The generated mesh is visually inspected and compared with SEM picture

in order to prevent high discrepancies between model and experiment.

## CONCLUSION

The remarkable properties of electrospun CNTs nanocomposites continue to draw attention in the development of multifunctional properties of nanostructures for many applications. The electrospinning process has extended with model for CNTs suspension behavior in the jet flow. Fiber diameter depend-

ence on electric field and solution estimated from experimental data. Multiscale model for calculation macroscopic mechanical properties for fibrous sheet is developed on two stages. Effective properties of the fiber at microscale are determined by homogenization using modified shear-lag model, while in the second stage the point-bonded stochastic fibrous network at mesoscale are replaced by continuum equivalent sheet. Elastic modulus and Poisson's ratio dependence on CNT volume concentration are calculated. Effective properties fibrous sheet as random stochastic network are determined analytically and numerically. We conclude that an addition of CNTs into the polymer solution results not always with significant improvement of rheological and structural properties.

## NOTATION

| | |
|---|---|
| $a$ | carbon nanotube radii |
| $a_i$ | orientation vector |
| $A$ | beam cross-section area |
| $c$ | spring constant |
| $C_{ij}$ | Cauchy-Green deformation tensor |
| $d$ | fiber diameter |
| $D_r$ | rotary diffusion |
| $D_{ijkl}$ | fourth order elastic tensor |
| $E$ | Young's modulus of elasticity |
| $E_f$ | elastic modulus of the carbon nanotube |
| $E_m$ | elastic modulus of the matrix |
| $E_\infty$ | externally imposed electric field |
| $f_i$ | volume fraction |
| $G$ | shear modulus |
| $I_1, I_2, I_3$ | invariants of the deformation tensor |
| $I$ | beam cross-section moment of inertia |
| $K$ | electrical conductivity |
| $k$ | Boltzmann constant |
| $\ell$ | carbon nanotube length |
| $n$ | dumbbells density |
| $p$ | unit vector |
| $R$ | matrix radii of CNT orientation |
| $\sigma_{rr}, \sigma_{\theta\theta}, \sigma_{zz},$ | components of stress tensor |
| $Q$ | configuration vector |
| $t$ | traction vector |
| $u$ | radial displacement |
| $U$ | strain energy density |
| $v$ | velocity vector |
| $V$ | electric field |
| $w$ | axial displacement |
| $\delta$ | Kronecker delta tensor |
| $\varepsilon_{rr}, \varepsilon_{\theta\theta}, \varepsilon_{rz}, \varepsilon_{zz},$ | components of strain tensor |
| $\langle\varepsilon_{ij}\rangle$ | macroscopic strain tensor |
| $\varepsilon_0$ | dielectric constant of the air |
| $\dot{\gamma}_{ij}$ | deformation rate tensor |
| $\gamma$ | surface tension |
| $\Theta$ | shape factor |
| $\kappa$ | shear-lag parameter |
| $\rho$ | fluid density |
| $\mu$ | surface charge density |
| $v, v_{12}, v_{21}$ | Poisson's ratio |
| $\omega_{ij}$ | vortices tensor |
| $\eta_s$ | solvent viscosity |
| $\Psi$ | probability distribution function |

## References

1. Ko, F. K.; Gogotsi, Y.; Ali, A.; Naguib, N.; Ye, H.; Yang, G.; Li, C.; Willis, P. Adv Mater 2003, 15, 1161.
2. Ye, H.; Lam, H.; Titchenal, N.; Gogotsi, Y.; Ko, F. Appl Phys Lett 2004, 85, 1775.
3. Xie, X. L.; Mai, Y. W.; Zhou, X. P. Mater Sci Eng R 2005, 49, 89.
4. Gojny, F. H.; Wichmann, M. H. G.; Fiedler, B.; Schulte, K. Compos Sci Technol 2005, 65, 2300.
5. Huang, Z. M.; Zhang, Y. Z.; Kotaki, M.; Ramakrishna, S. Compos Sci Technol 2003, 63, 2223.
6. Hohman, M. M.; Shin, M.; Rutledge, G.; Brenner, M. P. Phys Fluids 2001, 13, 2201.
7. Agic, A. Polimeri 2004, 25, 116 (in Croatian).
8. Kim, G. H. J Polym Sci Part B: Polym Phys 2006, 44, 1426.
9. Feng, J. J. Phys Fluids 2002, 14, 3912.
10. Song, Y. S.; Youn, J. R. Korea-Aust Rheol J 2004, 16, 201.
11. Keunings, R. Rheol Rev, to appear.
12. Forest, G. M., Zhou, R., Wang, Q. Int J Numer Anal Model 2007, 4, 478.
13. Myers, R. H.; Montgomery, D. C. Response Surface Methodology: Process and Product Optimization Using Designed Experiments. Wiley-Interscience: New York, 1995.
14. Gates, T. S.; Odegard, G. M.; Frankland, S. J. V.; Clancy, T. C. Compos Sci Technol 2005, 65, 2416.
15. Gao, X. L., Li, K. Int J Solids Struct 2005, 42, 1649.
16. Nairn, J. A. Adv Comput Lett 2004, 13, 6.
17. Yi, B. Y.; Berhan, L.; Sastry, A. M. J Appl Phys 2004, 96, 1318.
18. Cantournet, S.; Boyce, M. C.; Tsou, A. H. J Mech Phys Solids 2007, 55, 1321.
19. Zhigilei, L. V.; Wei, C.; Srivastava, D. Phys Rev B 2005, 71, 165417.
20. Silling, S. A.; Bobaru, F. Int J Non-Linear Mech 2005, 40, 395.
21. Berhan, L.; Yi, Y. B.; Sastry, A. M.; Munoz, E.; Selvidge, M.; Baughman, R. J Appl Phys 2004, 95, 4335.
22. Heyden, S. Ph. D. Dissertation, Lund University, 2003.
23. Dror, Y.; Salalha, W.; Khalfin, R. L.; Cohen, Y.; Yarin, A. L.; Zussman, E. Langmuir 2003, 19, 7012.
24. JSR RB. Publication. Syndiotactic 1,2-polybutadiene, JSR Corporation, TPE Div., Tokyo, Japan.
25. Agic, A.; Mijovic, B. J Text Inst 2006, 97, 419.
26. Eichhorn, S.; Sampson, W. W. J R Soc Interface 2005, 2, 309.